Int. J. Heat Mass Transfer. Vol. 13, pp. 1393–1414. Pergamon Press 1970. Printed in Great Britain

ENHANCEMENT OF DIFFUSION-LIMITED VAPORIZATION RATES BY CONDENSATION WITHIN THE THERMAL BOUNDARY LAYER
2. COMPARISON OF HOMOGENEOUS NUCLEATION THEORY WITH THE CRITICAL SUPERSATURATION MODEL†

MICHAEL EPSTEIN and DANIEL E. ROSNER‡

AeroChem Research Laboratories, Inc. (Subsidiary of Sybron Corporation), Princeton, New Jersey 08540

(*Received* 5 *December* 1968 *and in revised form* 1 *April* 1969)

Abstract—The validity of the critical supersaturation model (CSM) for predicting mass transfer effects of nonequilibrium fog formation in thermal boundary layers is examined by comparing CSM predictions with those of a more complete application of homogeneous nucleation theory to a simple flow with molecular transport. Expressions for the nucleation kinetics and droplet growth are combined with the steady one-dimensional conservation equations and suitably transformed to allow a digital computer solution of the vaporization of a hot condensed phase into a cold gaseous medium. Using a one dimensional film model of the thermal boundary layer, predictions of boundary layer profiles and the effects of nonequilibrium fog formation are obtained and, as anticipated by the CSM, the gross effect of fog formation is to significantly enhance the steady state vaporization rate. Our numerical calculations for methyl alcohol evaporation/condensation confirm the conceptual and computational utility of the critical supersaturation model for this class of problems, provided critical supersaturation predictions are based on large volumetric nucleation rates. Consistent with our purposes, the present investigation is limited to binary gas mixtures with (i) a Lewis number of unity and (ii) both mixture constituents of equal molecular weight. Since methyl alcohol vapor–air mixtures conform well to these restrictions, and are of interest in both research and technology, illustrative numerical results are given for this system.

NOMENCLATURE

B, mass-transfer number, equation (59);
c_c, local fog concentration (number density);
c_p, specific heat;
D, diffusion coefficient;
d, collision diameter, equation (5);
I_1, computer solution variable, equation (14);
I_2, computer solution variable, equation (15);
I_3, computer solution variable, equation (16);
J, volumetric steady-state nucleation rate;
k, Boltzmann constant;
L, latent heat of vaporization;
Le, Lewis number $D_v/[\lambda/(\rho_g c_p)]$;
$\mathscr{L}$, argument of tangency condition function, equation (41);
m, local mass fraction;

† Revised and extended version of AeroChem TP-192, November 1968. This research was supported in part by the U.S. Office of Scientific Research, Propulsion Division, under Contract AF 49(638)-1654. Based in part on a dissertation [24] submitted to the Faculty of the Polytechnic Institute of Brooklyn by M. Epstein in partial fulfillment of the requirements for the degree of Doctor of Philosophy (Mechanical Engineering), 1969.

‡ Present address: Department of Engineering and Applied Science, Yale University, New Haven, Connecticut 06520.

$\dot{m}''$, local mass flux;
$\dot{m}'''$, local mass rate of vapor consumption (per unit volume);
M, molecular weight;
N_A, Avogadro's number;
N, s_{crit} correlation constant, equation (28);
$\mathcal{N}$, argument of tangency condition function, equation (42);
p, pressure;
$\dot{q}''$, energy flux;
r_L, radius of growing droplet;
$\bar{r}_L$, radius of average size fog droplets;
r_{sep}, average separation between fog droplets;
r^*, critical drop radius, equation (2);
R, gas law constant;
s, supersaturation ratio, $p_v/p_{v,sat}(T)$;
$\mathcal{S}_{eff}$, argument of tangency condition function, equation (40);
t, time;
T, local absolute temperature;
v, mass average velocity of condensable vapor-inert gas mixture;
V, diffusion velocity;
y, distance from vaporizing surface;
Y, tangency condition function, equation (43).

Greek symbols

α_m, mass accommodation coefficient; equation (1) (assumed equal to α_{evap});
α_{th}, thermal accommodation coefficient, equation (16);
γ, ratio of specific heats;
δ_T, effective thickness of the thermal boundary layer;
ϵ, thickness of the free molecular layer for droplet growth, equation (5);
Δ, tangency condition function, equation (45);
λ, thermal conductivity of gas mixture;
$\bar{\lambda}$, average thermal conductivity of gas mixture in stagnant film;
ω, exponent in s_{crit} correlation, equation (28);
ρ, local density;
σ, liquid surface tension.

Subscripts

bp, boiling point;
c, fog or condensed (liquid) phase;
cn, condensation nucleii;
$crit$, values taken under a condition of appreciable nucleation;
i, inert gas;
L, bulk liquid phase;
max, maximum;
min, minimum;
n, at location of measurable nucleation;
nc, in the absence of homogeneous nucleation ($\dot{m}_c''' = 0$);
sat, thermodynamic saturation;
v, condensable vapor;
w, at phase boundary (vaporizing surface);
∞, in the free stream (cold boundary).

Miscellaneous

∇, Laplacian (differential operator).

1. INTRODUCTION

THEORETICAL studies of nonequilibrium condensation in fluid dynamic systems have been confined almost exclusively to the stepwise numerical calculation of vapor condensation in expansion nozzles, the major objective being to rationalize experimental data with existing theoretical expressions describing the rate of formation (nucleation) of particles of the new phase (see, e.g. [1, 2]). However, there is an entire class of problems in mass transfer theory in which "fog" nucleation is encountered but the fundamental mechanism of vapor transport is molecular diffusion rather than convection (e.g. fog formation† in (i) moist gas streams adjacent to cold surfaces, (ii) above heated fluids evaporating into cooler surroundings, (iii) metal-containing diffusion flames, etc.). Proper inclusion of nucleation phenomena into boundary layer treatments presents a formidable

† In the present context the terms fog, cloud, smoke, mist, fume, and aerosol are equivalent.

problem, due in part to the greatly increased complexity of the governing two-phase equations, coupled to the laws of condensation kinetics and particle growth. Recently reported measurements of the "anomalously high" vaporization rate of molten metals in cool surroundings [3, 4] have focused attention upon the mass transfer implications of condensation (fume formation) within thermal boundary layers. To explain the observed rates Hills and Szekely [5], and Turkdogan [6] proposed that vaporization rates are enhanced by vapor condensation in the steep temperature gradients surrounding the surface; i.e. since the nucleation of particles of the new phase occurs at the expense of the parent vapor concentration, the vapor concentration gradient at the vaporizing surface is increased. To predict the location of the "fog front", and hence the magnitude of the enhancement, Turkdogan [6] suggested a graphical-numerical model based on the notion that the supersaturation which causes appreciable nucleation (i.e. the so-called "critical supersaturation", s_{crit}, defined by a "critical nucleation rate") is locally achieved within the boundary layer. According to this model, the $s_{crit}(T)$ relation coupled with an estimate of the condensation-free vapor concentration profile, allows a rational prediction of the steady state vaporization rate in the presence of "fogging". This model, referred to hereafter as the "critical supersaturation model" (CSM), was analytically reformulated and generalized by Rosner [7], who obtained simple expressions for the vaporization rate in terms of a universal function implicitly containing the condensation kinetics. Collectively, these authors have shown that the CSM is in qualitative agreement with available experimental data, although these data are not yet precise or extensive.

In view of the present and future importance of this class of mass transfer phenomena, the main purpose of this investigation is to examine the validity of the CSM from a theoretical point of view. We hope to determine whether this seemingly *ad hoc* model offers a useful substitute for the more rigorous governing equations of mass transfer with condensation. To this end, we examine the condensation process via classical homogeneous nucleation theory in a deliberately simplified mass transfer system, using a numerical approach in which the governing conservation equations, suitably transformed, are rigorously solved on a digital computer. Mass-transfer rates predicted by the CSM are then compared with those obtained numerically. To facilitate this comparison, and to fix the underlying ideas and limitations of the CSM, we proceed along the lines of Rosner's treatment [7], introducing a few additional physical restrictions on the substances involved to embrace a wide spectrum of environmental conditions.

2. NUCLEATION AND DROPLET GROWTH

2.1 *Homogeneous nucleation kinetics*

To quantitatively understand the effects of nonequilibrium fog formation within thermal boundary layers, the rate of production (i.e. "birth rate") of liquid nuclei must be known. In the present study we exploit the classical theory of homogeneous nucleation from the vapor [8],† according to which density fluctuations (i.e. random collisions of vapor molecules) are responsible for the formation of condensation nuclei under supersaturated conditions. The number of droplets nucleated per unit volume per unit time, J, is then given by [8]:

$$J = \alpha_m \left(\frac{p_{v,sat}}{kT}\right)^2 \left(\frac{2\sigma M_v}{\pi N_A}\right)^{\frac{1}{2}} \frac{s^2}{\rho_L} \exp\left[-\frac{4\pi\sigma}{3kT} r^{*2}\right] \tag{1}$$

† In keeping with our objectives, we deliberately sidestep here the current controversy [9] over the validity of the classical theory (owing to its dependence on assumed macroscopic properties for the embryonic liquid phase). It is generally agreed that the classical theory of nucleation is qualitatively correct, and for some substances (e.g. methyl alcohol, investigated herein) the theory produces numerical results of sufficient accuracy for practical purposes.

where s is the local supersaturation ratio ($s \equiv p_v/p_{v,sat}$), α_m is the mass accommodation coefficient [10], and r^* is the radius of a droplet of critical size, given by

$$r^* = \frac{2M_v\sigma}{N_A\rho_L kT \ln s}. \tag{2}$$

It can be shown that equation (2) expresses an unstable equilibrium condition, between droplets of radius r^* and a supersaturated vapor phase, in that droplets of size $r < r^*$ tend to decrease in size while droplets of size $r > r^*$ grow indefinitely. For this reason the droplet of size r^* is defined as the condensation nucleus.

2.2 *Droplet growth*

Condensation nuclei grow by absorbing the surrounding vapor at a rate dependent on the prevailing supersaturation. Based on the notion of a vacuous layer (i.e. a region of the order of the mean free path of the gas mixture) surrounding a growing droplet, Fuchs [11] formulated a quasi-steady (Maxwell–Langmuir-type [12]) model that provides a smooth transition between free-molecular droplet growth (which occurs for droplet sizes appreciably smaller than the mean-free-path†) and continuum or diffusion-controlled droplet growth (for droplet sizes much larger than the mean-free-path). Kang [13] has recently extended the model to allow for the difference between the prevailing gas temperature and the droplet temperature. The resulting droplet growth expression is employed here in the following form:

$$\frac{dr_L}{dt} = \frac{s-1}{\dfrac{\rho_L(2\pi R_v T)^{\frac{1}{2}}}{\alpha_m p_{v,sat}} + \dfrac{\rho_L A L^2}{A R_v T^2} + \left[\dfrac{\rho_L R_v T}{p_{v,sat} D_v} + \dfrac{\rho_L A L^2}{R_v T^2 \lambda}\right]\left[\dfrac{r_L^2}{r_L + \epsilon}\right]} \tag{3}$$

where A is the slope of a linear approximation of the Clausius–Clapeyron equation for small $T_L - T$,[$A \approx 1{\cdot}3$ for $0 \leqslant L(T_L - T_\infty)/(R_v T_\infty^2) \leqslant 0{\cdot}7$]. The abovementioned temperature difference between droplet and surrounding vapor can be shown to be

$$T_L - T = \frac{\rho_L L}{\lambda}\left(1 + \frac{A}{\lambda}\cdot\frac{r_L^2}{r_L + \epsilon}\right)\frac{dr_L}{dt}. \tag{4}$$

In equations (3) and (4) ϵ is the vacuous layer thickness given by the mean-free-path of a vapor molecule moving among a mixture of inert gas and vapor molecules "frozen" in position; i.e.

$$\epsilon = \frac{kT}{\pi p[(d_v + d_i)/2]^2} \tag{5}$$

and A is defined by

$$A \equiv \left[\frac{(\gamma_v + 1)R_v}{2(\gamma_v - 1)}\right]\cdot\frac{[\alpha_m + (1 - \alpha_m)\alpha_{th,v}]\,p_v}{(2\pi R_v T)^{\frac{1}{2}}} + \left[\frac{(\gamma_i + 1)R_i}{2(\gamma_i - 1)}\right]\frac{\alpha_{th,i}p_i}{(2\pi R_i T)^{\frac{1}{2}}} \tag{6}$$

where α_{th} is the thermal accommodation coefficient [10].

† In the present class of problems condensation nuclei are some two orders of magnitude smaller than the mean free path.

3. COMPUTER SOLUTION OF NONEQUILIBRIUM CONDENSATION WITHIN THE THERMAL BOUNDARY LAYER

3.1 *Governing equations for a one-dimensional film*

To simplify matters, the steady state boundary layer will be represented by an equivalent "stagnant" film, which comprises the entire resistance to heat and mass transfer (see Fig. 1).

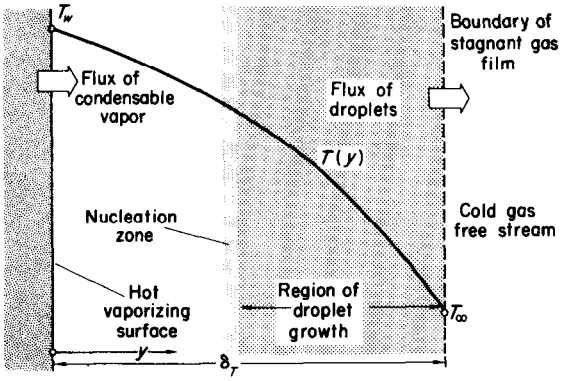

FIG. 1. Stagnant film model of nonequilibrium condensation within a thermal boundary layer.

Although this model is physically unrealistic in certain applications, its one-dimensional nature will allow us to retain all salient aspects of nucleation kinetics, particle growth and transport without severe mathematical repercussions.† In addition, this model has (i) already proved to be quite useful in correlating mass-transfer data for true boundary layers (see, e.g. [14]) and (ii) correctly represents certain one-dimensional experimental configurations used in fog nucleation research. Moreover, with regard to (i), rather than absolute predictions, our chief concern here is an appraisal of the CSM (see Introduction), and the stagnant film can be viewed as a reasonable mathematical artifice to accomplish this.

† As a droplet moves through the boundary layer it absorbs vapor in accord with its size, but its size is dependent on both its place of birth (nucleation) and the path it follows; therefore, that rate of condensed phase production is a function of droplet "history" as well as position. This complication, coupled with the multi-dimensional character of most boundary layers, results in a formidable mathematical and computational problem.

The one-dimensional flow system (Fig. 1) will be restricted to a fluid containing three components, viz. inert gas, condensed phase (in the form of fog), and parent vapor. The mean separation of droplets in the fog will be assumed to be sufficiently great (compared with their radii) that the droplets may be considered non-interacting. Hence, the growth behavior of each droplet is that of an isolated particle, where the local gas properties are identified with the properties at a "large distance" from the droplet. Consequently, droplets influence each other only through their combined influence on the surrounding gaseous medium. At any location droplets may be found varying in size, velocity, and temperature according to their histories. By assuming a large number of droplets, and suitably defining local average fog properties (density, temperature, etc.), the motions of the non-interacting droplets can be shown to correspond to the motions of a continuum [15].

We identify the mass of the condensed phase per unit spatial volume by ρ_c, and, neglecting the volume occupied by the droplets, the inert gas density is ρ_i. With respect to this same spatial volume the parent vapor density is ρ_v. In this manner, we can express the overall density, ρ, of the three component mixtures as $\rho = \rho_g + \rho_c$, where ρ_g is the density of the binary gas mixture consisting of the condensable vapor and the inert gas (hereafter referred to as the "gas mixture") given by $\rho_g = \rho_i + \rho_v$. In the usual manner, we introduce the mass fractions of the vapor and the inert gas, in the *gas* mixture, viz. $m_v \equiv \rho_v/\rho_g$ and $m_i \equiv \rho_i/\rho_g$ respectively. It is also convenient to define a local fog mass fraction, viz.

$$m_c \equiv \rho_c/\rho. \tag{7}$$

For slow flows, with which we are dealing here, the momentum equation reveals the total pressure, p, to be constant. When radiant heat transfer and thermal diffusion are neglected, and the specific heats of the vapor and liquid phase components are assumed constant, the energy and vapor species conservation

equations, integrated once, can be shown to take the following forms:

$$\lambda \frac{dT}{dy} = \dot{m}_v'' c_{p,v} T - \dot{m}_v'' m_c \times [L - c_{p,L}(T_L - T)] - \dot{q}'' \quad (8)$$

$$\rho_g D_v \frac{dm_v}{dy} = -\dot{m}_v'' \cdot (1 - m_v) \cdot (1 - m_c) \quad (9)$$

where T_L is the local, average, droplet temperature, and $\dot{q}''$ and $\dot{m}_v''$ are constants of integration identifiable with the total energy and mass flux ($\dot{m}_v'' = \rho v$) leaving the vaporizing surface. The condensed phase species conservation equation can be formally written

$$\dot{m}_v'' \frac{dm_c}{dy} = \dot{m}_c''' \quad (10)$$

where it has been assumed that the droplets do not *diffuse*, but are convected with the local mass average velocity† of the gas mixture, v. It is well known that droplets with radii smaller than $\approx 10^{-6}$ cm (i.e. comparable to the dimensions of condensation nuclei) exhibit considerable Brownian movement. However, as shown later in our numerical example (Section 3.2), nuclei grow so quickly through the diffusion stage that it seems highly unlikely that Brownian motion will yield a significant contribution to the transport of fog.

To complete the system of equations [equations (8)–(10)] it remains to specify the condensed phase "source" term, $\dot{m}_c'''$. As a result of the Stefan flow, droplets are convected in the positive y-direction (see Fig. 1). The size of a droplet located at y, due to nucleation at location $\xi (0 \leqslant \xi \leqslant y)$ is

$$r_L(y) = r^*(\xi) + \int_{r^*(\xi)}^{r_L(y)} dr_L = r^*(\xi) + \int_\xi^y \frac{1}{v} \frac{dr_L}{dt} d\psi \quad (11)$$

where r^* is the radius of a liquid nucleus [see equation (2)]. The mass of the droplet at y is $\frac{4}{3}\pi\rho_L r_L^3(y)$, and the number of droplets nucleated per cubic volume per s at ξ is $J(\xi)$; therefore, since the flux of droplets at y due to nucleation at ξ is $J(\xi)\,d\xi$, in the absence of droplet coalescence the mass flux at y due to nucleation at ξ is $\frac{4}{3}\pi\rho_L r_L^3(y)\,J(\xi)\,.\,d\xi$. The total mass flux of droplets, $\dot{m}_c''$, at y is the sum of contributions from all locations ξ such that $0 \leqslant \xi \leqslant y$; i.e.

$$\dot{m}_c''(y) = \tfrac{4}{3}\pi\rho_L \int_0^y \left[r^*(\xi) + \int_\xi^y \frac{1}{v} \frac{dr_L}{dt} d\psi \right]^3 \times J(\xi)\,d\xi. \quad (12)$$

Since $\dot{m}_c''' = d\dot{m}_c''/dy$, the condensed phase production term is explicitly

$$\dot{m}_c'''(y) = 4\pi\rho_L \cdot \frac{1}{v} \cdot \frac{dr_L}{dt} \int_0^y \left[r^*(\xi) + \int_\xi^y \frac{1}{v} \frac{dr_L}{dt} d\psi \right]^2 J(\xi)\,d\xi + \tfrac{4}{3}\pi\rho_L r^{*3} J \quad (13)$$

In view of the form of $\dot{m}_c'''$, the condensed phase species conservation equation [equation (10)] is an *integro-differential* equation. Fortunately, however, by defining the following auxiliary dependent variables, this equation can be reduced to a coupled system of ordinary differential equations:

$$I_1(y) \equiv 4\pi\rho_L \int_0^y \left[r^*(\xi) + \int_\xi^y \frac{1}{v} \frac{dr_L}{dt} d\psi \right]^2 J(\xi) d\xi \quad (14)$$

† In the "stagnant" film the mass average velocity is due entirely to the Stefan flow (interfacial flow). In the case of vaporization, it is directed away from the vaporizing surface. Again, in keeping with our objectives, we do not consider here gravitational sedimentation of the largest droplets relative to the Stefan flow.

$$I_2(y) \equiv 8\pi\rho_L \int_0^y \left[r^*(\xi) + \int_\xi^y \frac{1}{v}\frac{\mathrm{d}r_L}{\mathrm{d}t}\,\mathrm{d}\psi \right] J(\xi)\,\mathrm{d}\xi \quad (15)$$

$$I_3(y) \equiv 8\pi\rho_L \int_0^y J(\xi)\,.\,\mathrm{d}\xi. \quad (16)$$

Therefore, the final form of the conservation equations [equations (8)–(10)] describing vaporization into a stagnant film in the presence of homogeneous nucleation, may be written as follows:†

$$\frac{\mathrm{d}T}{\mathrm{d}y} = -\frac{\dot{m}_v'' c_{p,v}}{\lambda}\left\{\left[\frac{L}{c_{p,v}} - \frac{c_{p,L}}{c_{p,v}}(T_L - T)\right] m_c + \frac{\dot{q}''}{\dot{m}_v'' c_{p,v}} - T\right\} \quad (17)$$

$$\frac{\mathrm{d}m_v}{\mathrm{d}y} = -\frac{1}{Le}\cdot\frac{\dot{m}_v'' c_{p,v}}{\lambda}(1 - m_v)\,.\,(1 - m_c) \quad (18)$$

$$\frac{\mathrm{d}m_c}{\mathrm{d}y} = \frac{1}{\dot{m}_v''}\left(\frac{\rho}{\dot{m}_v''}\frac{\mathrm{d}r_L}{\mathrm{d}t} I_1 + \tfrac{4}{3}\pi\rho_L r^{*3} J\right) \quad (19)$$

$$\frac{\mathrm{d}I_1}{\mathrm{d}y} = \frac{\rho}{\dot{m}_v''}\frac{\mathrm{d}r_L}{\mathrm{d}t} I_2 + 4\pi\rho_L r^{*2} J \quad (20)$$

$$\frac{\mathrm{d}I_2}{\mathrm{d}y} = \frac{\rho}{\dot{m}_v''}\frac{\mathrm{d}r_L}{\mathrm{d}t} I_3 + 8\pi\rho_L r^* J \quad (21)$$

$$\frac{\mathrm{d}I_3}{\mathrm{d}y} = 8\pi\rho_L J \quad (22)$$

where the mass average velocity, v, has been replaced by $\dot{m}_v''/\rho$. The overall density, ρ, is related to the dependent variables of equations (17)–(22) by the following form of the ideal equation of state:

$$\rho = \frac{p}{R_i T}\left(\frac{1}{1 - m_c}\right)\left\{\frac{1}{1 + [(M_i/M_v) - 1]\,m_v}\right\}. \quad (23)$$

The above conservation equations are seen to consist of a boundary value problem [equations (17) and (18), subject to $T = T_w$ and $m_v = m_{v,w}$ at $y = 0$, and $T = T_\infty$ and $m_v = m_{v,\infty}$ at $y = \delta_T$] coupled to an initial value problem [equations (19)–(22), subject to $m_c = I_1 = I_2 = I_3 = 0$ at $y = 0$]. Since equations (17) and (18) are of first order and have four boundary conditions, the vaporization flux, $\dot{m}_v''$, and the heat flux, $\dot{q}''$, are eigenvalues of the equations.

In equations (17)–(22) J and $\mathrm{d}r_L/\mathrm{d}t$ are determined by nucleation theory (Section 2.1) and droplet growth theory (Section 2.2). However, droplet growth theory cannot be immediately applied without further discussion. It can be seen from equation (3) that the droplet growth rate is a function of droplet size, especially for larger droplets. Now at any particular location within the fog there will be droplets of different sizes; consequently, to meaningfully include equation (3) in the present form of the conservation equations, a suitable average droplet size, $\bar{r}_L$, is employed here. The *arithmetic* mean droplet radius† can be calculated by considering the total flux of droplet radii at location y, viz.

$$\int_0^y \left[r^*(\xi) + \int_\xi^y \frac{1}{v}\frac{\mathrm{d}r_L}{\mathrm{d}t}\,\mathrm{d}\psi \right] . J(\xi)\,\mathrm{d}\xi.$$

Dividing this term by the total number flux of droplets at location y, $\int_0^y J(\xi)\,\mathrm{d}\xi$, and using definitions (15) and (16), we find the arithmetic mean droplet radius to be

$$\bar{r}_L(y) = I_2(y)/I_3(y). \quad (24)$$

† See the nomenclature for remaining definitions.

† Of course, other mean droplet size definitions exist—the three most commonly used being the mean according to droplet surface area and volume, and the (Sauter) volume/surface mean. The logical choice in any given application is determined by the characteristics of fogs of particular importance. Fuchs [16] recommends the arithmetic mean radius for describing the rate of evaporation of fogs, and the surface-averaged mean to describe their optical density. In the present investigation, we have found that the various averages do not differ very much from each other (< 10 per cent deviation), hence our results should be unaffected by this arbitrariness. If information on particle size *distribution* is necessary, or if the particle cloud is extremely dilute, then the fog *cannot* be regarded as a continuous medium and must be locally described by a particle size distribution function. Under such circumstances, the droplet cloud continuum equation [equation (10)] must be replaced by a Boltzmann-like equation for non-interacting particles.

Finally, it is of interest to present expressions descriptive of important properties of the fog. The *fog concentration* (in units of droplets per unit volume) can be shown to be

$$c_c(y) = \frac{1}{8\pi\rho_L(\mathrm{d}r_L/\mathrm{d}t)}\left(\frac{\mathrm{d}I_2}{\mathrm{d}y} - r^*\frac{\mathrm{d}I_3}{\mathrm{d}y}\right). \quad (25)$$

The ratio of the spatial volume to the volume occupied by the average size droplet is easily obtained from equation (25) as

$$\left(\frac{r_{sep}}{\bar{r}_L}\right)^3 = \frac{6\rho_L}{\bar{r}_L^3}\cdot\frac{\mathrm{d}r_L}{\mathrm{d}t}\cdot\frac{1}{(\mathrm{d}I_2/\mathrm{d}y) - r^*(\mathrm{d}I_3/\mathrm{d}y)} \quad (26)$$

where r_{sep} is the average separation between droplets. According to our underlying assumptions, the droplet concentration must be large enough for the fog to behave as a continuum, and the volume occupied by the droplets must be negligible (i.e. the separation between droplets must be large compared with their radii).

To this level of approximation equations (17)–(22) govern the condensing flow of any vapor in a "stagnant" film. While it is not possible to integrate them analytically, it is possible to carry out numerical computations in any system for which the relevant properties of the vapor and condensate are known or estimable. Results of such computations are discussed below.

3.2 *Nonequilibrium condensation of methyl alcohol in the stagnant film*

Digital computer solutions of equations (17)–(22) were obtained for the vaporization of liquid methyl alcohol into air. Numerical techniques and physical data used in the calculations are outlined in Appendices A and B. Calculations were made for several liquid surface temperatures, T_w, and for a constant free stream temperature, T_∞, of 175°K (see Fig. 1), the latter coinciding approximately with the freezing point of methyl alcohol. The concentration of methyl alcohol vapor at the outer edge of the stagnant film (i.e. the "free stream") was taken to be zero. The thermal stagnant film thickness, δ_T, was arbitrarily set equal to 0·01 cm.†

To simplify the numerical solution and to provide a basis for a comparison with the theory presented in Section 4, the following additional assumptions were made:

A3.1 The mass fraction of the vapor at the vaporizing surface is equal to the saturation mass fraction at the surface temperature.
A3.2 The local thermal conductivity, λ of the gas mixture can be replaced by a constant average conductivity, $\bar{\lambda}$, within the film.
A3.3 The temperature difference between the fog and the gas mixture, $T_L - T$, can be neglected.
A3.4 The Lewis number, Le, is unity.
A3.5 The latent heat of vaporization, L, is constant.

Assumption A3.1 has been discussed extensively in the literature (see, e.g. [7, 17]), and it has been shown that only at very high mass-transfer rates is there a significant departure from equilibrium at the surface. Assumption A3.2 has proved extremely useful in indicating basic trends in combustion theory and, in the present problem, will permit straightforward comparisons with predictions of the CSM. From the results of the numerical solution and equation (4), the maximum value of $T_L - T$ is found to be of the order of 4 K, therefore validating A3.3 *a posteriori*. Few binary gas mixtures violate the condition $Le = 1$ to any great extent, and the approximation is especially

† Techniques for evaluating meaningful film thicknesses in any particular environment are discussed throughout mass-transfer literature (see, e.g. [14]). In the numerical calculations it turns out that the *dimensionless* vaporization rate $\dot{m}_v'' c_{p,v}\delta_T/\bar{\lambda}$ (discussed in detail in Section 4.4) only increases by approximately 8 per cent for a change in δ_T from 0·01 to 1·0 cm. Consideration of possible competitive vapor removal by foreign condensation nucleii indicates that thin boundary layers are less likely to be influenced by naturally occurring aerosol concentrations. In the present case, the concentration level of foreign nucleii necessary to strongly influence vapor removal in the film [which can be shown to be of the order of $(2\pi\, d_{cn}\delta_T^2)^{-1}$] would exceed those naturally occurring ($\approx 10^4 - 10^5$ cm^{-3} of ≈ 1 μ dia. particles) by more than 2 orders of magnitude.

good for methyl alcohol/air mixtures (for $0 \leqslant m_v \leqslant 0{\cdot}1$, Le remains within 5 per cent of unity). Finally, regarding A3.5, the latent heat is generally a weak function of temperature, and by choosing a suitable average value, the variation in L for methyl alcohol throughout the stagnant film is only 8 per cent.

A typical picture of the predicted nucleation zone structure is presented in Figs. 2 and 3 for $T_w = 277$ K. Figure 2 reveals that within the nucleation zone the radius of the average size droplet, $\bar{r}_L$, is about an order of magnitude greater than the critical nucleation radius ($r^* \approx 10^{-7}$ cm or 10 Å). The arithmetic mean droplet size leaving the nucleation zone is of the order of $\bar{r}_L = 10^{-5}$ cm, and the largest droplet (nucleated at the position where $J = 1$ nucleus cm^{-3} sec^{-1}) grows to a size of $r_{L,\max} = 5 \times 10^{-5}$ cm. Since the mean free path throughout the stagnant film is approximately 6×10^{-6} cm the droplets are predicted to grow very rapidly to sizes greater than the mean free path, consistent with our neglect of Brownian motion† and the use of a droplet growth theory that accounts for the transition region (Section 2.2). In Fig. 3, it is seen that all properties vary monotonically across the nucleation zone, except, of course, for the nucleation rate, J, and the supersaturation ratio s. It appears that noticeable condensation does not occur until s reaches a certain critical value at which J increases rapidly with small corresponding changes in s. The same phenomenon is observed in supersonic nozzles and expansion cloud chambers, where the value of s consistent with an appreciable condensation effect is referred to as the "critical supersaturation", s_{crit}. As noted below, the near constancy of s

† Further estimates making use of the final results, the application of Fick's law [viz. $c_c V_c = -D_c(dc_c/dy)$] to the Brownian motion of fog droplets, and the Stokes–Einstein relation (see [18]) for the computation of the effective droplet diffusion coefficient, D_c, in the gas mixture shows that one is justified in neglecting fog diffusion. The diffusion velocity of the fog, V_c, based on the average size particle within the nucleation zone, was found to be less that $\frac{1}{10}$ of the mass average velocity.

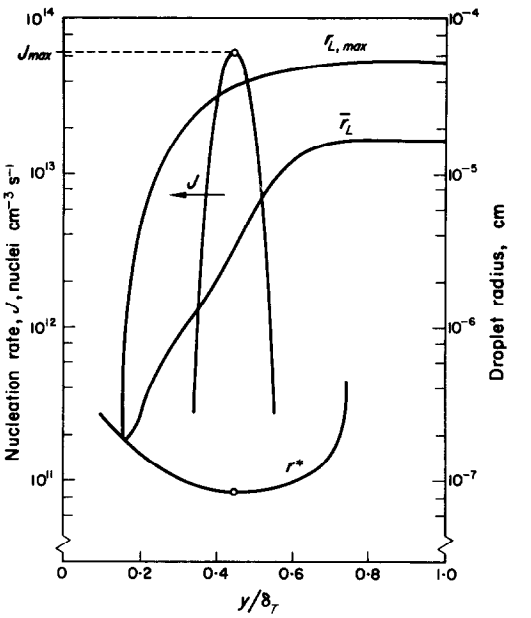

FIG. 2. Typical variations of pertinent droplet sizes within the thermal film in the presence of homogeneous nucleation (vaporization of CH_3OH into air: $T_w = 227°$ K, $T_\infty = 175°$ K, $p = 1$ atm, $\delta_T = 0{\cdot}01$ cm).

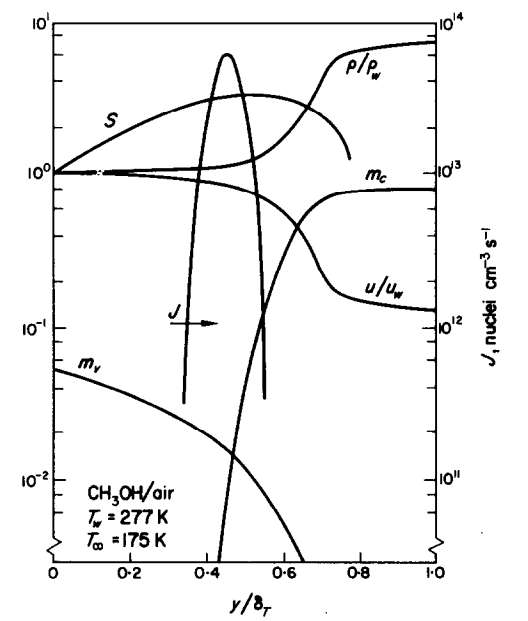

FIG. 3. Typical property variations within the thermal film in the presence of homogeneous nucleation (vaporization of CH_3OH into air: $T_w = 277$ K, $T_\infty = 175$ K, $p = 1$ atm, $\delta_T = 0{\cdot}01$ cm).

within the nucleation zone is a basis of the CSM (Section 4).

Temperature profiles in the stagnant film are shown in Fig. 4. Deviation from the usual linear profiles (found in a source-free stagnant film) is primarily due to the release of latent heat as the vapor condenses.† Table 1 presents

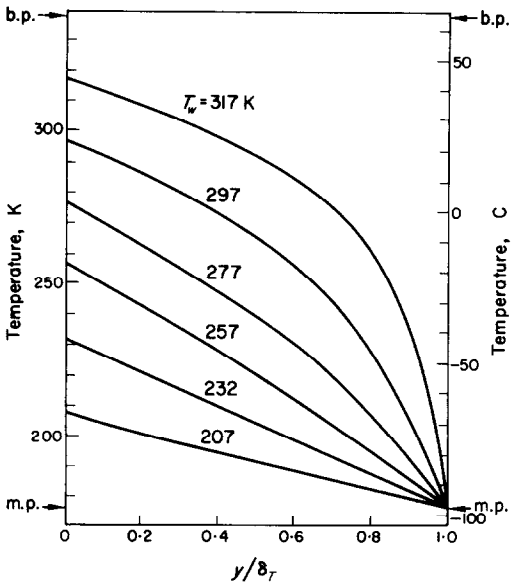

FIG. 4. Temperature profiles within the thermal film in the presence of homogeneous nucleation (CH_3OH/air: T_∞ = 175 K, p = 1 atm, δ_T = 0·01 cm).

the maximum nucleation rate, J_{max}, for several surface temperatures. The numerical calculations reveal the nucleation rates to be extremely high, even at surface temperatures such that the vapor concentration within the film is everywhere small. Finally, it should be mentioned that a typical methyl alcohol fog in the stagnant film may contain 10^{10} droplets cm^{-3} of average size $\bar{r}_L = 10^{-5}$ cm, each droplet separated by about 20 $\bar{r}_L$. These results justify the treatment of the fog as a dilute particle continuum.

Thus far, we have said nothing about the net vaporization rate, $\dot{m}_v''$. Naturally, the vaporization rate and the structure of the nucleation zone are interrelated; i.e. the solution of equations (17)–(22) depends on the numerical value of $\dot{m}_v''$ However, it will be convenient to postpone discussion of $\dot{m}_v''$ until the CSM is introduced. This simplified physical model, yielding basic $\dot{m}_v''$ trends rather than detailed nucleation zone structure, avoids the numerical solution of the complete set of governing equations in predicting values of $\dot{m}_v''$. By applying this model to the vaporization of methyl alcohol, it is now possible to test its validity, as well as to examine the effect of nonequilibrium condensation on the vaporization rate.

Table 1. Maximum nucleation rate in the boundary layer

(T_∞ = 175 °K, p = 1 atm, δ_T = 0·01 cm)

T_w (°K)	J (nuclei cm^{-3} s^{-1})
207	$5{\cdot}99 \times 10^{-4}$
222	$1{\cdot}27 \times 10^{10}$
232	$3{\cdot}45 \times 10^{11}$
257	$1{\cdot}49 \times 10^{13}$
277	$6{\cdot}37 \times 10^{13}$
297	$1{\cdot}26 \times 10^{14}$
317	$8{\cdot}77 \times 10^{16}$

4. THE CRITICAL SUPERSATURATION MODEL OF MASS TRANSFER IN THE PRESENCE OF NONEQUILIBRIUM VAPOR CONDENSATION

4.1 *Estimation and extrapolation of critical supersaturation data*

The sensitive relation between s and J is clearly illustrated in Fig. 5 for water vapor. Suppose, for a configuration like that shown in Fig. 1, we guess at the nucleation rate corresponding to an appreciable condensation effect; e.g. for H_2O vapor at 0°C, we take an appreciable nucleation rate to be, say, J_{crit} = 10^2 nuclei cm^{-3} s^{-1}.† The critical supersaturation ratio, s_{crit}, for this nucleation rate is 4·47.

† At high surface temperatures ($T_w \to T_{bp}$) the net mass transfer also exerts an appreciable influence on the temperature profile.

† The subscript "*crit*" refers to values taken at the location of measurable condensation. The nucleation rate J_{crit} (discussed in Section 3.2) is approximately equal to J_{max}.

Had we chosen an appreciable nucleation rate to be as high as 10^4 or as low as 1, we would have arrived at a critical supersaturation between 4·22 and 4·78. Therefore, an uncertainty of even a few orders of magnitude in the value of

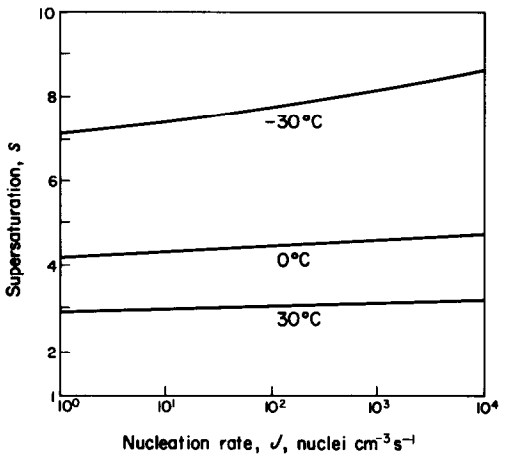

FIG. 5. Nucleation rates from Frenkel's equation [(1) and (2)], for H_2O.

J_{crit} has relatively little effect on the corresponding value of s_{crit}.†

Typical critical supersaturation data for various substances are shown in Fig. 6. These data were obtained by substituting an assumed value of J_{crit} into the following form of Frenkel's equation, equations (1) and (2):

$$2[\ln s_{crit}]^3 + \left\{\ln\left[\alpha_m\left(\frac{p_{v,sat}}{T}\right)^2\frac{(\sigma M_v)^{\frac{1}{2}}}{\rho_L}\right] + 59{\cdot}82 - \ln J_{crit}\right\}.[\ln s_{crit}]^2 - 17{\cdot}49\left(\frac{\sigma}{T}\right)^3\left(\frac{M_v}{\rho_L}\right)^2 = 0 \qquad (27)$$

where $p_{v,sat}$ is expressed in torr and all other quantities are in c.g.s. units. The physical data used in obtaining these curves are collected in Appendix B; however, it should be remarked

† Since J varies linearly with α_m [see equation (1)], the same conclusion applies to an uncertainty in the value of the mass accomodation coefficient.

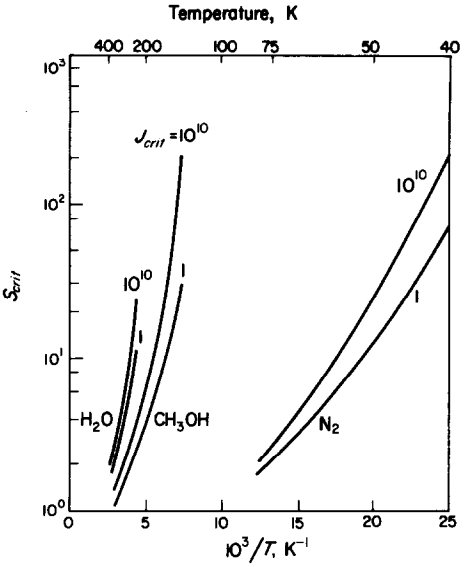

FIG. 6. Critical supersaturation predictions from Frenkel's equation [(1) and (2)] for H_2O, CH_3OH and N_2.

that all the physical quantities are based on the formation of *liquid* nuclei, even at temperatures well below the equilibrium freezing point.‡

The s_{crit} vs. T data can be correlated reasonably well by the formula

$$\ln s_{crit} = \text{const} + [N/(R_v T)]^{\omega} \qquad (28)$$

where N is a constant. For example, the curves shown in Fig. 6, for a choice of $J_{crit} = 1$ nucleus $cm^{-3}\ s^{-1}$, can be accurately represented as follows:

$$CH_3OH\ \ln s_{crit} = -0{\cdot}134 + (236/T)^{2{\cdot}37} \qquad 137 < T < 337\ K \qquad (29)$$

$$H_2O\ \ln s_{crit} = -0{\cdot}228 + (340/T)^{2{\cdot}35} \qquad 228 < T < 373\ K \qquad (30)$$

$$N_2\ \ln s_{crit} = -0{\cdot}688 + (90/T)^{1{\cdot}99} \qquad 50 < T < 77\ K. \qquad (31)$$

‡ Clusters of a supersaturated vapor, in an environment considerably lower in temperature than the equilibrium freezing point of the condensing substance, first form by homogeneous nucleation into droplets of a supercooled liquid. Only thereafter are these supercooled droplets crystallized.

Critical supersaturation data obtained in cloud chamber experiments support the above linear variation of ln s_{crit} with $T^{-\omega}$. Although most investigators conclude that ω is of the order of $\frac{3}{2}$; in fact, some experimenters report that ln s_{crit} varies linearly with T^{-1} (see [19] for a summary of this work). The reason for this discrepancy probably lies in the relatively smaller temperature ranges over which the experimental results were obtained. In certain limited temperature ranges, the power ω in equation (28) can be substantially reduced. For example, by expanding the last term in equation (30) in a Taylor series about $T = 268$ K, the s_{crit} expression for H_2O takes the following approximate form:

$$\ln s_{crit} = -2{\cdot}59 + (1100/T) \qquad (230 < T < 300\,\text{K}). \qquad (32)$$

It follows from the above discussion that only a limited knowledge of the actual nucleation rate is sufficient to extrapolate reasonable absolute values of s_{crit} and its temperature variation. This fact forms the foundation of the critical supersaturation model.

4.2 *The critical supersaturation model (CSM) of mass transfer—generalized and extended*

Suppose, in the presence of a large temperature gradient, the vapor being transported across the thermal boundary layer is observed to undergo homogeneous nucleation to the liquid phase (see Fig. 7).† The vaporizing surface is located at $y = 0$, and at $y = y_n$ a measurable nucleation effect is observed. Within the nucleation zone the pressure exerted by the condensing vapor is dictated by equation (27), thus, according to the discussion in Section 4.1, the vapor pressure (based on a reasonable choice of J_{crit})

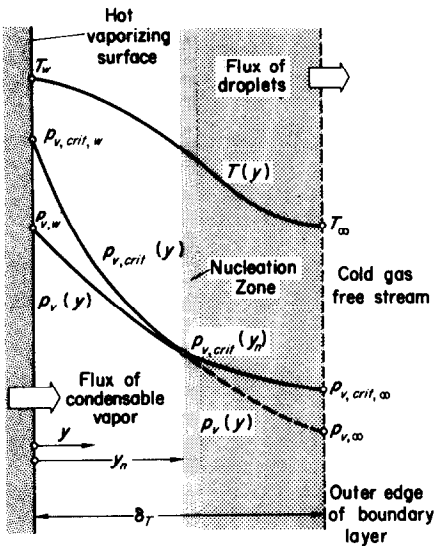

FIG. 7. Critical supersaturation model (CSM) of mass transfer in the presence of nonequilibrium condensation.

is approximately $p_{v,crit} = p_{v,sat} \cdot s_{crit}$. Hence, at location $y = y_n$ the following two physical constraints must be imposed on the vapor concentration profile:

$$p_v(y_n) = p_{v,crit}(y_n) \qquad (33)$$

$$\left(\frac{\partial p_v}{\partial y}\right)_{y=y_n} = \left(\frac{\partial p_{v,crit}}{\partial y}\right)_{y=y_n}. \qquad (34)$$

Equation (33) simply re-expresses the physical existence of the critical supersaturation. The second constraint treats point y_n as a "match" point where the vapor pressure profile outside the nucleation zone is smoothly joined to the vapor pressure profile within the nucleation zone; i.e. equation (34) is the physical condition that fulfills the continuity of $\partial p_v/\partial y$ and, hence, continuity of the vapor diffusion flux throughout the boundary layer. In essence, equations (33) and (34) constitute the critical supersaturation model, which is essentially equivalent to representing the vapor pressure profile in the nucleation zone by $p_{v,crit}(y)$.

From a mathematical standpoint, equations (33) and (34) may be viewed as a boundary condition on the vapor concentration profile at

† It will be assumed here that the vapor is moving outward from a liquid or solid surface into the adjacent boundary layer (vaporization or sublimation); however, the following argument is also applicable to the case where the vapor is transported from the free stream into the boundary layer (i.e. surface condensation). An application of the CSM to predict incipient fog formation near cool surfaces is presented in [20].

the point of appreciable nucleation. It should be pointed out that since the location of the nucleation zone is unknown and can only be determined as part of the solution, conditions (33) and (34) are equivalent only to a single boundary condition. This boundary condition will hereafter be referred to as the "tangency condition".

To analytically reformulate the tangency condition in terms of properties of the evaporating liquid (or solid) surface, we retain assumptions A3.2–A3.5, and add the following assumptions:

A4.1 The "products" of the condensation process, viz. the droplets,† are not directed towards the vaporizing surface but, instead, move in the positive y-direction and eventually leave the boundary layer (see Fig. 7).

A4.2 The molecular weights of the mixture components are approximately equal.

Assumption A4.1 is justified only for specific geometries and is valid in the configuration considered in Fig. 1.‡ The region $0 < y < y_n$ therefore constitutes a "source-free" region. The error due to A4.2 can obviously be quite large when the condensing vapor has a very different molecular weight from that of the inert gas through which it is transported [e.g. Fe(g)/He(g)]. This is especially true when $T_w \to T_{bp}$ (i.e. at high vaporization rates). However, to facilitate the comparisons of interest here this assumption proves convenient.§

By combining A4.1, A4.2, A3.4, we obtain the well known heat-mass transfer analogy in the region between the vaporizing surface and he nucleation zone, viz.

$$\frac{m_v - m_v(y_n)}{m_{v,w} - m_v(y_n)} = \frac{T - T(y_n)}{T_w - T(y_n)}. \tag{35}$$

Since $M_i \approx M_v$ [A4.2], equation (35) may be written in terms of the vapor pressure; i.e.

$$\frac{p_v - p_v(y_n)}{p_{v,w} - p_v(y_n)} = \frac{T - T(y_n)}{T_w - T(y_n)}. \tag{36}$$

Differentiating both sides of equation (36) with respect to the distance y, and invoking equations (33) and (34), we have

$$\left(\frac{\partial p_{v,crit}}{\partial y}\right)_{y=y_n} = \frac{p_{v,w} - p_{v,crit}(y_n)}{T_w - T(y_n)} \left(\frac{\partial T}{\partial y}\right)_{y=y_n} \tag{37}$$

Now, in view of A3.5, the Clausius–Clapeyron equation can be written:

$$p_{v,sat} = \text{const} \cdot \exp\left(-\frac{L}{R_v T}\right). \tag{38}$$

Accordingly, the *critical vapor pressure* can be expressed as [see equation (28)]

$$p_{v,crit} = \text{const} \cdot \exp\left\{-\left[\frac{L}{R_v T} - \left(\frac{N}{R_v T}\right)^{\omega}\right]\right\} \tag{39}$$

In terms of the dimensionless constants††

$$\mathscr{S}_{eff} \equiv p_{v,crit}(T_w)/p_{v,w} \tag{40}$$

$$\mathscr{L} \equiv L/(R_v T_w) \tag{41}$$

† As in Section 3, the vaporizing surface is in an inert gas environment so that the only "reaction" with which we have to contend is nucleation of the condensed phase.

‡ Certainly the effect of droplet motion in the direction of the vaporizing surface can hardly be ignored when considering vaporization phenomena in, for example, a forward stagnation point or rotating disk boundary layer (cf. e.g. D. R. Olander and R. Omberg. Paper presented at 64th *AIChE* Mtg., 13–22 March 1969, New Orleans, La.). Nevertheless, this assumption permits such considerable mathematical simplification it is worth including in the formulation, even at the expense of limiting the applicability of the tangency condition by ruling out certain boundary layer geometries.

§ Considering the fact that $M_{CH_3OH} = 32{\cdot}04$ and $M_{air} = 28{\cdot}97$, one can understand the choice of a methyl alcohol vapor–air mixture for illustrative calculations. Additionally, methyl alcohol vapor is largely unassociated in the saturated state, and its nucleation behavior (which has been studied experimentally [26]) conforms well to the predictions of classical nucleation theory.

†† If $p_{v,w} = p_{v,sat}(T_w)$, then $\mathscr{S}_{eff} = s_{crit}(T_w)$.

$$\mathcal{N} \equiv [N/(R_v T_w)]^{\omega} \tag{42}$$

and the dimensionless nucleation zone temperature

$$Y \equiv [T_w - T(y_n)]/T_w \tag{43}$$

the tangency condition [equation (37)] takes the following dimensionless form:

$$\exp\left[\mathcal{L}\frac{Y}{1-Y} - \mathcal{N}\frac{1-(1-Y)^{\omega}}{(1-Y)^{\omega}}\right] = \mathcal{S}_{eff}\left[1 + \mathcal{L}\frac{Y}{(1-Y)^2} - \omega\mathcal{N}\frac{Y}{(1-Y)^{\omega+1}}\right]. \tag{44}$$

The solution of this transcendental equation provides the temperature in the nucleation zone, $T(y_n)$, as a function of the properties evaluated at the vaporizing surface. In problems of mass transfer we are mainly concerned with the concentration gradient; thus a useful dimensionless parameter is:

$$\Delta \equiv \frac{m_{v,w}}{T_w}\cdot\frac{(\partial T/\partial y)_{y=0}}{(\partial m_v/\partial y)_{y=0}} = \frac{p_{v,w}}{T_w}\,\frac{(\partial T/\partial y)_{y=0}}{(\partial p_v/\partial y)_{y=0}}. \tag{45}$$

Equations (36) and (44) show that Δ is related to Y by

$$\Delta = Y + \frac{(1-Y)^{\omega+1}}{\mathcal{L}(1-Y)^{\omega-1} - \omega\mathcal{N}}. \tag{46}$$

Inspection of equation (46) shows that Δ, as well as Y, are functions only of the properties of the vaporizing surface. The functions $\Delta(\mathcal{L}, \mathcal{N}, \mathcal{S}_{eff}, \omega)$ and $Y(\mathcal{L}, \mathcal{N}, \mathcal{S}_{eff}, \omega)$ will be referred to as the tangency condition functions.†

† For negligible interfacial mass velocity but $M_i \neq M_v$, Rosner [7] first derived equations (44) and (46) for the particular case $\omega = 1$. In this singular case, Δ is a universal function of only *two* parameters, viz. $\mathcal{L} - \mathcal{N}$ and $\mathcal{S}_{eff}$, and is shown plotted in [7, 20]. Although the tangency condition represented by equations (44) and (46) is based on an analytical form [equation (28)] that best correlates s_{crit} data, it clearly does not permit the remarkable degree of simplicity given by Rosner's ($\omega = 1$) form. However, to facilitate a fair comparison between the CSM and the numerical solution of the governing equations, equations (44) and (46) will be employed in this investigation.

4.3 *The enhanced mass-transfer rate for the case of vaporization and nonequilibrium condensation*

Equation (45) reveals that the CSM provides a relation between the mass-transfer rate and the heat-transfer rate (through the function Δ, which incorporates all effects of nonequilibrium condensation kinetics). However, this model alone does not provide sufficient information to calculate the vaporization rate, i.e. some additional knowledge of the temperature profile must be invoked. Fortunately, the unity Lewis number assumption enables us to do this, and thus obtain an analytic expression for the mass-transfer rate of the condensable vapor applicable not only for stagnant one-dimensional films but also for arbitrary mass transfer systems (boundary layers subject to A4.1, A4.2). Again, we consider the flow of a condensable vapor-inert gas mixture, together with the condensed phase in the form of a fog (treated as a continuum moving with the mass-average velocity of the gas phase in which the temperature difference between the fog and the gas mixture is neglected). The conservation equations [equations (8)–(10)] may be rewritten in vector notation as follows:

$$\nabla\cdot\left(\frac{\lambda}{c_{p,v}}\nabla T\right) - \dot{\mathbf{m}}''\cdot\nabla T = -\frac{\dot{m}_c'''L}{c_{p,v}} \tag{47}$$

for energy transfer† and

$$\nabla\cdot[D_v\rho_g\nabla m_v + \dot{\mathbf{m}}''(1 - m_v - m_c + m_v m_c)] = 0 \tag{48}$$

$$\nabla\cdot[m_c\dot{\mathbf{m}}''] = \dot{m}_c''' \tag{49}$$

for mass transfer. Now, assuming $m_v m_c \ll [1 - m_v - m_c]$;‡ and utilizing the overall continuity equation governing the total mass flux (viz.

† This simplified form of the energy equation is valid only when the specific heats of the inert gas and condensable vapor are equal.

‡ The validity of this assumption for the methyl alcohol–air mixture in the stagnant film is apparent from *a posteriori* examination of the numerical solution in Section 3.2, which reveals that the ratio $m_v m_c/(1 - m_v - m_c)$ never exceeds $1{\cdot}4 \times 10^{-2}$.

$\nabla . \dot{\mathbf{m}}'' = 0$) and equation (49), the condensable vapor species conservation equation [equation (48)] becomes

$$\nabla . (D\rho_g \nabla m_v) - \dot{\mathbf{m}}'' . \nabla m_v = \dot{m}_c''' . \quad (50)$$

Invoking $Le \approx 1$ in the above equation and eliminating the local rate of fog production, $\dot{m}_c'''$, between the resulting equation and equation (47), we obtain the following differential equation for the "composite" dependent variable $T + (m_v L/c_{p,v})$:

$$\nabla . \left[\frac{\lambda}{c_{p,v}} \nabla \left(T + \frac{L}{c_{p,v}} m_v \right) \right] - \dot{\mathbf{m}}'' . \nabla \left(T + \frac{L}{c_{p,v}} m_v \right) = 0. \quad (51)$$

Therefore, subject to the assumptions made, $T + (m_v L/c_{p,v})$ obeys a conservation equation of exactly the same form as those governing heat and/or mass transfer in non-condensing environments (i.e. when $\dot{m}_c''' = 0$). Accordingly, we can write the following similarity relationship in the boundary layer:

$$\frac{T + (m_v L/c_{p,v}) - [T_w + (m_{v,w} L/c_{p,v})]}{T_\infty + (m_{v,\infty} L/c_{p,v}) - [T_w + (m_{v,w} L/c_{p,v})]} = \frac{(m_v)_{nc} - m_{v,w}}{m_{v,\infty} - m_{v,w}} \quad (52)$$

where $(m_v)_{nc}$ is the local vapor mass fraction in the absence of condensation, but with all mass-transfer conditions (including the total mass flux $\dot{\mathbf{m}}''$) being the same as in the presence of condensation. Differentiating equation (52) with respect to y, the temperature gradient at the vaporizing surface is found to be

$$\left(\frac{\partial T}{\partial y} \right)_{y=0} = \frac{T_w - T_\infty + (L/c_{p,v})(m_{v,w} - m_{v,\infty})}{m_{v,w} - m_{v,\infty}} \times \left(\frac{\partial m_v}{\partial y} \right)_{y=0;nc} - \frac{L}{c_{p,v}} \left(\frac{\partial m_v}{\partial y} \right)_{y=0} . \quad (53)$$

From equation (45), the concentration gradient at the vaporizing surface in the presence of nonequilibrium condensation is immediately obtained:

$$\frac{(\partial m_v/\partial y)_{y=0}}{(\partial m_v/\partial y)_{y=0;nc}} = \frac{[(m_{v,w} - m_{v,\infty}) L/(c_{p,v} T_w)] + [1 - T_\infty/T_w)]}{[\Delta . (\dot{m}_{v,w} - m_{v,\infty})/m_{v,w}] + [(m_{v,w} - m_{v,\infty}) L/(c_{p,v} T_w)]} \quad (54)$$

where $(\partial m_v/\partial y)_{y=0;nc}$ is the concentration gradient at the vaporizing surface in the absence of condensation, but with all mass-transfer conditions (including $\dot{m}''$) the same.

If the interfacial velocity is small (i.e. negligible Stefan flow), the left-hand side of equation (54) is simply the vaporization enhancement due to nonequilibrium condensation within the thermal boundary layer, where condensation kinetics have been included through the tangency condition function, Δ. Suppose, however, that the condensation process occurs everywhere in local thermodynamic equilibrium. Then, the vapor pressure throughout the boundary layer is dictated by the Clausius–Clapeyron equation [equation (38)]. Differentiating equation (38) with respect to y and evaluating the result at the vaporizing surface we obtain:

$$\mathscr{L}^{-1} = \frac{p_{v,sat}(T_w)}{T_w} \cdot \frac{(\partial T/\partial y)_{y=0}}{(\partial p_{v,sat}/\partial y)_{y=0}} . \quad (55)$$

By comparing this relation with equation (45), we see that one need only replace Δ by $\mathscr{L}^{-1}$ stagnant film is immediately obtained from equations (56) and (57)‡:

$$\frac{\dot{m}_v'' c_{p,v}\delta_T}{\bar{\lambda}} = \ln\left\{1 + \frac{[(m_{v,w} - m_{v,\infty})\, L/(c_{p,v}T_w)] + [1 - (T_\infty/T_w)]}{[\Delta\cdot(1 - m_{v,w})/m_{v,w}] + [(1 - m_{v,w})\, L/(c_{p,v}T_w)]}\right\} \tag{58}$$

in equation (54) to obtain the vaporization enhancement when local equilibrium governs the condensation process. This is seen to be a particular case (first derived by Hills and Szekely [5]†) of the nonequilibrium generalization obtained here [equation (54)].

4.4 *Comparison of the critical supersaturation model with the computer solution*

In order to compare the CSM with the more detailed analysis given in Section 3, including the effects of the Stefan flow and latent heat release, we again consider the simple geometry of the stagnant film system. In the absence of chemical or physical change, the steady state concentration profile in the film of thickness δ_T is given by

$$\frac{(m_v)_{nc} - m_{v,w}}{m_{v,\infty} - m_{v,w}} = \frac{\exp(\dot{m}_v'' c_{p,v} y/\bar{\lambda}) - 1}{\exp(\dot{m}_v'' c_{p,v}\delta_T/\bar{\lambda}) - 1} \tag{56}$$

where $\dot{m}_v''$ is the total mass flux throughout the stagnant film. Now, in the case of the stagnant film the total mass flux is equal to the vaporization rate; consequently, $\dot{m}_v''$ must necessarily equal the vaporization rate in the presence of condensation within the stagnant film, in order to maintain the required correspondence between mass-transfer conditions. Now, at the vaporizing surface the net flux of inert gas is zero, hence we have the following condition

$$\frac{\dot{m}_v'' c_{p,v}}{\bar{\lambda}} = \frac{-(\mathrm{d}m_v/\mathrm{d}y)_{y=0}}{1 - m_{v,w}}. \tag{57}$$

Introducing condensation kinetics through equation (54), the enhanced vaporization rate in the where [cf. A3.1] $m_{v,w} = m_{v,sat}(T_w)$. Interestingly enough, we see that the CSM, reformulated and generalized as suggested by Rosner [7], predicts a vaporization relation paralleling the familar stagnant film result:

$$\dot{m}_v'' c_{p,v}\delta_T/\bar{\lambda} = \ln(1 + B) \tag{59}$$

where B is referred to as the "mass transfer number" or mass transfer "driving force". In a stagnant film free of vapor sinks (i.e. $\dot{m}_c''' = 0$) B is given by $(m_{v,w} - m_{v,\infty})/(1 - m_{v,w})$, and the corresponding vaporization rate will be referred to as the minimum (or non-enhanced) vaporization rate for the stagnant film, viz. $[\dot{m}_v'' c_{p,v}\delta_T/\bar{\lambda}]_{\min}$.

Before proceeding with a comparison of the CSM with the computer solution it is of interest to consider the predicted *location* of the nucleation zone. This can be accomplished by considering the temperature profile in the source-free region of the stagnant film ($0 < y < y_n$; $m_c = 0$):

$$\frac{T - T_w}{T_n - T_w} = \frac{\exp(\dot{m}_v'' c_{p,v} y/\bar{\lambda}) - 1}{\exp(\dot{m}_v'' c_{p,v} y_n/\bar{\lambda}) - 1}. \tag{60}$$

Substituting equations (57) and (60) into definition (45) and utilizing definition (43), we find:

$$\frac{y_n}{\delta_T} = \left(\frac{\dot{m}_v'' c_{p,v}\delta_T}{\bar{\lambda}}\right)^{-1} \times \ln\left[1 + \frac{m_{v,sat}(T_w)}{1 - m_{v,sat}(T_w)}\cdot\frac{\bar{Y}}{\Delta}\right] \tag{61}$$

where $\dot{m}_v'' c_{p,v}\delta_T/\bar{\lambda}$ is given by equation (58).

† While not explicitly indicated by Hills and Szekely [5, 21], to apply their equilibrium results in systems with an appreciable contribution of condensate to the local mass flux, one must add the abovementioned restriction on $m_v m_c$.

‡ Equation (58) reveals $\dot{m}_v'' c_{p,v}\delta_T/\bar{\lambda}$ to be independent of the film thickness δ_T [cf. Section 3.2]. Interestingly enough, this CSM result [eq. (58) and its limiting cases] can be shown to apply equally well to the quasi-steady vaporization of a macroscopic *droplet* [24], provided one replaces δ_T by the instantaneous droplet *radius*.

To visualize the influence of homogeneous nucleation on mass transfer in the stagnant film, the dimensionless vaporization enhancement, $\dot{m}_v''/(\dot{m}_v'')_{\min}$ and nucleation zone location, y_n/δ_T, are shown in Fig. 8 for the vaporization of liquid methyl alcohol into air. The vaporization enhancement, starting from unity when the fog first appears at a finite distance from the vaporizing surface ($y_n/\delta_T = Y/\Delta$), increases with increasing T_w, reaching a maximum value when the nucleation zone takes a position closest to the vaporizing surface. With further increases in T_w, the enhancement ratio decreases toward unity, and the nucleation zone moves away from the wall, eventually leaving the film (when $T_w = T_{bp}$). Thus, at high surface temperatures the latent heat release terms dominate the nucleation kinetic term, and the mass transfer number in equation (58) reduces to that for minimum vaporization.† The s_{crit} data used in obtaining the curves exhibited in Fig. 8 correspond to $J_{crit} = 1$ and $J_{crit} = 10^{12}$ nuclei cm^{-3} s^{-1}.‡ In reference to the numerical solution data shown in the figure, y_n/δ_T represents that point in the film where the nucleation rate attains its maximum value, $J_{\max}$ [see Fig. 2].

Agreement between the numerical solution and the CSM is seen to be good, provided the CSM predictions are based on "realistic" values of J_{crit}. If a highly nonphysical choice of J_{crit} is made, the model no longer represents a useful approximation to the rigorous solution of the governing equations. The results of the numerical calculations for methyl alcohol (presented in Table 1) indicated that the best choice of J_{crit} is any value between 10^{10} and 10^{17} nuclei cm^{-3} s^{-1}. Numerical calculations of nonequilibrium condensation in supersonic nozzles also lead to J_{crit} criteria of this magnitude, e.g., Duff and Hill [1] have shown that a nucleation rate of $J \approx 10^{16}$ nuclei cm^{-3} s^{-1} for carbon dioxide corresponds to a measurable condensation effect on nozzle pressure distribution. Similar results were obtain by Griffin and Sherman [2] for expanding nitrogen, copper, and zinc vapors; and by Head [22] for water vapor. At present, however, there seens to be no simple method for predicting the order of magnitude of J_{crit} in novel mass transfer situations, which can be regarded as an intrinsic shortcoming of the CSM.

Mention should be made of the fact that small values of J_{crit} provide useful predictions of when measureable fogging effects first appear in a mass-transfer system.§ In Fig. 8 this is indicated

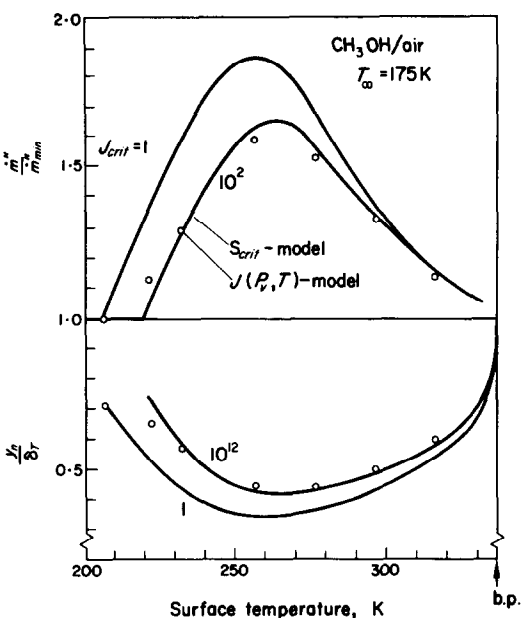

FIG. 8. Vaporization enhancements and nucleation zone position [CH_3OH/air: $T_\infty = 175$ K, $p = 1$ atm, $m_{v,\infty} = 0$; $\delta_T = 10^{-2}$ cm (for J-model)].

† Although there is considerable scatter in the existing experimental data, vaporization rates reported by Turkodogan and Mills [3] seem to verify the diminishing enhancement effect at high surface temperatures (see, also [7, 21]).

‡ In addition to the s_{crit} correlation for $J_{crit} = 1$ nuclei cm^{-3} s^{-1}, equation (29), the following correlation was extrapolated from equation (27) for methyl alcohol:

$$\ln s_{crit} = -0{\cdot}0508 + (255/T)^{2{\cdot}49} \qquad (J_{crit} = 10^{12}).$$

§ In [20] a value of $J_{crit} = 1$ nuclei cm^{-3} s^{-1} was employed in the prediction of incipient fog formation conditions.

by the "shift" in the appropriate value of J_{crit} at low wall temperatures, reflecting a rapidly decreasing nucleation rate in this region (see Table 1).

5. CONCLUSIONS

The critical supersaturation model (CSM) provides a simple closed form expression [equation (54)] for condensation-enhanced vaporization rates in real boundary layers, in terms of a single function, Δ which incorporates condensation kinetics. In addition, this result encompasses the special (limiting) case of condensation at local thermodynamic equilibrium. By applying the expression to the stagnant film system, we have shown that the model predicts enhanced vaporization rates consistent with a more complete theoretical model over a wide range of vaporizing liquid surface temperatures. While it is impossible to claim that this agreement between the CSM and the more complete theoretical model can be reproduced with *any* homogeneous nucleation expression, without further computations it is safe to assume that similar agreement will be found whenever the nucleation expression displays "critical supersaturation" (i.e. threshold) behaviour, as demanded by experiment.

However, while capable of revealing some important mass-transfer trends, the CSM provides no information on condensation zone *structure* and the important question of *particle size distribution*. While it is, thus, only a small step into a new area of considerable research potential, further theoretical studies would appear to be premature in the absence of more extensive and precise data. It is recognized that many of the assumptions [e.g. A4.1 and A4.2] exploited here will not apply in specific mass-transport systems.† Nevertheless the present model provides a useful analytical basis for understanding more complex situations. Most important, the present analysis has revealed that selection of physically meaningful J_{crit} (i.e. the actual nucleation rate, J_{max}, to within, say, four orders of magnitude) is sufficient for accurate CSM predictions of vaporization enhancements. Although the seemingly arbitrary choice $J_{crit} = 1$ nucleus $cm^{-3}\ s^{-1}$ has proven to be a useful criterion in the prediction of *incipient* fog formation conditions,‡ more complete computer solutions indicate that a much larger J_{crit} is appropriate in the study of enhanced vaporization effects. There is some indirect evidence substantiating $J_{crit} \approx 10^{15}$ nuclei $cm^{-3}\ s^{-1}$ (see Section 4.4) as a relevant criterion for s_{crit} in some systems; however, a method of selecting a physically meaningful J_{crit} *a priori* (i.e. in terms of known parameters of the mass-transfer problem) would constitute a useful next step.

ACKNOWLEDGEMENTS

We wish to thank Dr. D. R. Olander, R. Omberg, Dr. J. Szekely, Dr. G. M. Pound and Dr. S. C. Kurzius for their helpful discussions of aspects of this work.

REFERENCES

1. K. M. Duff and P. G. Hill, Condensation of carbon dioxide in supersonic nozzles, *Proceedings of the Heat Transfer and Fluid Mechanics Institute*, pp. 268–294. Stanford University Press (1966).
2. J. L. Griffin and P. M. Sherman, Computer analysis of condensation in highly expanded flows, *AIAA Jl* **3**, 1813 (1965).
3. E. T. Turkdogan and K. C. Mills, The theory of enhancement of diffusion-limited vaporization rates by a condensation process—Part II, experimental, *Trans. Am. Inst. Min. Engrs* **230**, 750 (1964).
4. G. W. Toop and F. D. Richardson, Reactions between levitated drops of metal and flowing gases, presented at the Symposium on Extractive Metallurgy (April 1967), British Inst. Min. and Metallurgy, Preprint 9.
5. A. W. D. Hills and J. Szekely, Notes on vaporization into much colder surroundings, *Chem. Engng Sci.* **19**, 79 (1964).

† Interestingly enough, in the zirconium droplet combustion experiments of L. Nelson and H. S. Levine (*High Temp. Sci.*, **1**, in press) it appears that oxide vapor nucleation, coagulation and particulate recapture by the parent droplet *suppresses* the net vaporization loss of zirconium in oxygen/rare gas ambients.

‡ The criterion $J_{crit} = 1$ nucleus $cm^{-3}\ s^{-1}$ has been used extensively in comparing theoretical nucleation rate expressions with supersaturation data obtained in cloud chambers [19].

6. E. T. TURKDOGAN, The theory of enhancement of diffusion-limited vaporization rates by a convection-condensation process—Part I, theoretical, *Trans. Am. Inst. Min. Engrs* **230**, 740 (1964).
7. D. E. ROSNER, Enhancement of diffusion-limited vaporization rates by condensation within the thermal boundary layer—1. The critical supersaturation approximation, *Int. J. Heat Mass Transfer* **10**, 1267 (1967); For extensions of this work, and the correction of typographical errors, see also: D. E. ROSNER and M. EPSTEIN, Condensation-enhanced vaporization rates in nonisothermal systems, *Trans. Met. Soc. AIME* **242**, 2355 (1968).
8. J. FRENKEL, *Kinetic Theory of Liquids*. Oxford University Press, London (1946).
9. H. REISS, The statistical mechanical theory of irreversible condensation—I, *J. Chem. Phys.* **20**, 1216 (1952).
10. B. PAUL, Compilation of evaporation coefficients, *ARS Jl* **32**, 1321 (1962).
11. N. A. FUCHS, *Evaporation and Droplet Growth in Gaseous Media*. Pergamon Press, Oxford (1959).
12. I. LANGMUIR, Dissociation of hydrogen into atoms—II, *J. Am. Chem. Soc.* **37**, 417 (1915).
13. S. KANG, Analysis of condensation droplet growth in rarefied and continuum environments, *AIAA Jl* **5**, 1288 (1967).
14. B. R. BIRD, W. E. STEWART and E. N. LIGHTFOOT, *Transport Phenomena*. John Wiley, New York (1960).
15. F. E. MARBLE, Dynamics of a gas containing small solid particles, *Combustion and Propulsion*, Fifth AGARD Colloquium, High Temperature Phenomena, pp. 175–215. Pergamon Press, Oxford (1963).
16. N. A. FUCHS, *The Mechanics of Aerosols*. U.S. Dept. of Commerce Office of Technical Services, Washington, D.C. (1959).
17. L. N. TUNG and H. G. DRICKAMER, Diffusion through an interface, *J. Chem. Phys.* **20**, 6 (1952).
18. S. K. FRIEDLANDER, Particle diffusion in low-speed flows, *J. Colloid Interface Sci.* **23**, 157 (1967).
19. W. J. DUNNING, Experimental methods for the study of nucleation and condensation, AIAA Progress in Astronautics and Aeronautics: *Heterogeneous Combustion*, Vol. 15, pp. 739–761. Academic Press, New York (1964).
20. D. E. ROSNER and M. EPSTEIN, Fog formation conditions near cool surfaces, *J. Colloid Interface Sci.* **28**, 60 (1968).
21. A. W. D. HILLS and J. SZEKELY, A note on the enhancement of the diffusion-limited vaporization rates by condensation within the thermal boundary layer, *Int. J. Heat Mass Transfer* **12**, 111–114 (1969).
22. R. M. HEAD, Investigations of spontaneous condensation phenomena, Ph.D. Thesis, C.I.T., Pasadena California (1949).
23. S. GILL, A process for the step-by-step integration of differential equations in an automatic digital computing machine, *Proc. Camb. Phil. Soc.* **47**, 96 (1951).
24. M. EPSTEIN, Nonequilibrium fog formation within the thermal boundary layer, Ph.D. Dissertation, Polytechnic Institute of Brooklyn, Brooklyn, New York (1969).
25. R. P. SHUTT, A theory of diffusion cloud chambers, *Rev. Scient. Instrum.* **22**, 730 (1951).
26. J. L. KATZ and B. J. OSTERMIER, Diffusion cloud chamber investigation of homogeneous nucleation, *J. Chem. Phys.* **47**, 478 (1967).
27. *Handbook of Chemistry and Physics*, 47th Ed. The Chemical Rubber Publishing Co., Cleveland, Ohio (1966–67).
28. N. V. TSEDERBERG, *Thermal Conductivities of Gases and Liquids*. M.I.T. Press, Cambridge, Massachusetts (1965).

APPENDIX A

Numerical Solution of Equations (17)–(22)

Due to the functional complexity of the nucleation rate, J, equations (17)–(22) constitute a highly nonlinear system of ordinary differential equations. The system may be viewed as a boundary value problem, consisting of equation (17) and (18), in which the local mass fraction of condensate, m_c, is a source term. The value of m_c is determined by the solution of the initial-value problem composed of equations (19)–(22). The boundary-value problem is coupled to the initial-value problem through the vapor mass fraction, m_v, the temperature, T, and the mass flux, $\dot{m}_v''$.

Our method of solution consisted of estimating (via the CSM) the values of $\dot{m}_v''$ and $\dot{q}''$ and then systematically refining these estimates so that the resulting trial solution satisfies the boundary conditions. For each set of trial eigenvalues, the boundary-value system [(17) and (18)], along with (19)–(22), is treated as an initial-value problem, starting from $y = 0$ and integrating towards $y = \delta_T$. Iterative schemes have been developed for this method (known as the "shooting" method) that depend on each integration reaching the end of the interval, $y = \delta_T$. Unfortunately, the value of $m_v(\delta_T)$ was found to be extremely sensitive to the values of $\dot{m}_v''$ and $\dot{q}''$, and the integration could not be carried to the end of the interval unless the eigenvalues were correct to four decimal places. Therefore, this class of iterative techniques was not practical.

To overcome this difficulty, the integrations were carried out in stages in the y direction.

This method is greatly facilitated by the following two simplifications: First, by eliminating the liquid condensate mass fraction, m_c, between equations (17) and (18), a relation between the two eigenvalues can be derived,† viz.

$$\frac{\dot{m}_v'' c_{p,v} \delta_T}{\bar{\lambda}} = \ln\left\{1 + \frac{(L/c_{p,v})\,[m_{v,w} - m_{v,\infty}] + (T_w - T_\infty)}{[\dot{q}''/(\dot{m}_v'' c_{p,v})] - T_w + (L/c_{p,v})\,[1 - m_{v,w}]}\right\}$$

and consequently a guess at only one eigenvalue is required for each integration. Second, as already indicated, the CSM provides a rational first estimate of the vaporization rate, $\dot{m}_v''$ (to within an accuracy of some 5 per cent). Two solutions, with corresponding eigenvalues $\dot{m}_{v,\mathrm{I}}''$ and $\dot{m}_{v,\mathrm{II}}''$ are integrated to such a point that the behavior of the m_v profile clearly indicates whether the required solution lies between them or not. If not, other solutions are evaluated until a pair is found between which the required solution does lie. From the behavior of m_v, an estimate is then made of the fraction $f(0 < f < 1)$ such the $\dot{m}_{v,\mathrm{I}}'' + f(\dot{m}_{v,\mathrm{II}}'' - \dot{m}_{v,\mathrm{I}}'')$ is a fair approximation of the eigenvalue corresponding to the desired solution. A third solution is then started, not from $y = 0$ but from some larger value y_1 of y at which the value of m_v does not change between integrations by more than 0·001 (times an appropriate power of 10). Depending on the behavior of the third solution, either another solution is started from y_1 or a solution is started by interpolating between $\dot{m}_{v,\mathrm{III}}''$ and $\dot{m}_{v,\mathrm{I}}''$ or $\dot{m}_{v,\mathrm{II}}''$ at a point y_2 further out in the interval. Many forward integrations are required (usually between 15 and 20) before $y = \delta_T$ is reached.

Each forward integration was carried out by the Runge–Kutta fourth-order method, as developed by Gill [23]. The effects of rounding errors were found to be large so that it was necessary to retain up to 16 decimal places in the integration. A step size of 0·01 δ_T was chosen so as to yield a small truncation error. The calculations were executed on an IBM 360 digital computer at the computer center of the Polytechnic Institute of Brooklyn.

† It should be noted that additional assumptions are implicit in this relation, viz. that the Lewis number is unity and the product $m_v m_c$ is negligible compared with the term $1 - m_v - m_c$. Justification for these assumptions (for a methyl alcohol vapor–air mixture) appears in Sections 3.2 and 4.3.

APPENDIX B

Property Values of CH_3OH and Air

In this appendix pertinent physical properties of methyl alcohol and air are listed for the temperature range 175–320 K.† When necessary, the expressions for $p_{sat}(T)$, $\sigma(T)$, and $\rho_L(T)$ were assumed valid for the liquid phase at temperatures below the triple point. The thermal accomodation coefficients of methyl alcohol vapor and air (relative to a liquid methyl alcohol surface) were taken as 1·0 in the absence of information suggesting more appropriate values. All vapor pressures and temperatures are in units of Torr (mm Hg) and degrees Kelvin, respectively.

Methyl alcohol (M = 32·04):

$$\ln p_{sat} = 20{\cdot}53 - (4700/T) \qquad [25]$$

$$\sigma = 48{\cdot}58 - 0{\cdot}0882\,T,\ \mathrm{g\,s^{-2}} \qquad [25]$$

$$\rho_L = 1{\cdot}032 - (7{\cdot}013 \times 10^{-4})T - (4{\cdot}1 \times 10^{-7})T^2,\ \mathrm{g\,cm^{-3}} \qquad [26]$$

$$\lambda = (2{\cdot}575 \times 10^{-5}) - (1{\cdot}216 \times 10^{-7})T + (5{\cdot}22 \times 10^{-10})T^2,\ \mathrm{cal\,cm^{-1}\,s^{-1}\,K^{-1}} \qquad [26]$$

† Physical properties of water and nitrogen can be found in [24].

$D = 0{\cdot}133(T/273)^{2{\cdot}0}$, $cm^2\ s^{-1}$ (for CH_3OH/air) [25]
$c_p = 0{\cdot}3277$, cal $g^{-1}\ K^{-1}$ [26]
$L = 291{\cdot}5$, cal g^{-1} (from expression for p_{sat}) —
$d = 4{\cdot}43 \times 10^{-8}$, cm (from viscosity data) [27]
$\alpha_m = 0{\cdot}045$ [10]
$\alpha_{th} = 1{\cdot}0$ —

Air ($M = 28{\cdot}97$):
$\lambda = 5{\cdot}74 \times 10^{-5}(T/273)^{0{\cdot}856}$, cal $cm^{-1}\ s^{-1}\ °K^{-1}$ [27]
$d = 3{\cdot}32 \times 10^{-8}$, cm (from viscosity data) [27]
$\gamma = 1{\cdot}41$
$\alpha_{th} = 1{\cdot}0$.

The following arithmetic mean conductivity, $\bar{\lambda}$, was employed in the numerical integration of the conservation equations (Section 3.2):

$$\bar{\lambda} = (\lambda_w + \lambda_\infty)/2$$

where the mixture thermal conductivity was based on the following simplified form of the Wassiljewa equation [28]:

$$\lambda \approx \frac{(m_v/M_v)\,\lambda_v + (m_i/M_i)\,\lambda_i}{(m_v/M_v) \quad (m_i/M_i)}.$$

RENFORCEMENT DES VITESSES DE VAPORISATION LIMITEÉ PAR LA DIFFUSION PAR LA CONDENSATION À L'INTÉRIEUM DE LA COUCHE LIMITE THERMIQUE—2. COMPARAISON DE LA THÉORIE DE LA NUCLÉATION HOMOGÈNE AVEC LE MODÉLE DE LA SURSATURATION CRITIQUE

Résumé—La validité du modèle de la sursaturation critique (CSM) pour la prévision des effets de transport de masse de la formation de brouillard en non-équilibre dans des couches limites thermiques est examiné comparant les prévisions CSM avec celles d'une application plus complète de la théorie de la nucléation homogène à un écoulement simple avec transport moléculaire. Les expressions pour la cinetique de la nucléation et la croissance des gouttelettes sont combinées avec les équations de conservation permanentes et unidimensionnelles et transformées convenablement pour permettre une solution au calculateur numérique de la vaporisation d'une phase condensée chaude dans un milieu gazeux froid. En employant un modèle de film unidimensionnel de la couche limite thermique, on obtient des prévisions des profils de couche limite et les effets de la formation de brouillard en non-équilibre et, comme il a été prévu par le CSM, l'effet principal de la formation de brouillard est de renforcer sensiblement le flux de vaporisation en régime permanent. Nos calculs numériques pour l'évaporation et la condensation de l'alcool méthylique confirment l'utilité comme concept et pour le calcul du modèle de sursaturation critique pour cette classe de problèmes, pourvu que les prévisions de sursaturation critique soient basées sur de grandes vitesses de nucléation volumiques. L'étude actuelle est limitée, ce qui est compatible avec nos buts, aux mélanges gazeux binaires avec:

(1°) un nombre de Lewis égal à l'unité et,
(2°) des constituants du mélange avec des masses moléculaires égales. Puisque les mélanges air–alcool méthylique se conforment bien à ces restrictions et sont intéressantes à la fois pour la recherche et la technólogie, on donne pour ce système des résultats numériques illstratifs.

STEIGERUNG DER DIFFUSIONSBEGRENZTEN VERDAMPFUNGSGESCHWINDIGKEITEN DURCH KONDENSATION INNERHALB DER WÄRMEGRENZSCHICHT 2. VERGLEICH DER HOMOGENEN KRISTALLISATIONSKERNBILDUNGSTHEORIE MIT DEM KRITISCHEN SUPERSATURATIONSMODELL

Zusammenfassung—Die Gültigkeit des Modells der kritischen Übersättigung (MkÜ) für die Voraussage des Einflusses von Stoffübertrangung auf die instationäre Nebelbildung in thermischen Grenzschichten wird geprüft. Zu diesem Zweck werden Voraussagen des MkÜ mit solchen einer geneueren Anwendung der homogenen Keimbildungstheorie auf eine Strömung mit moleckularem Transport verglichen. Ausdrücke für die Kinetik der Keimbildung und für das Tropenwachstum werden stationären, eindeimensionalen Erhaltungssätzen kombiniert und für eine Berechnung auf einem Digitalcomputer transformiert. Damit werden Lösungen für die Verdampfung einer heissen flüssigen Phase in ein kaltes gasförmiges Medium

erhalten. Unter Verwendung eines eindimensionalen Filmmodells für die thermische Grenzschicht werden Voraussagen für die Grenzschictprofile und die Einflüsse von instantionärer Nebelbildung erhalten.

Es ergibt sich, ebenso wie bei dem MkÜ, dass der wesentliche Einfluss der Nebelbildung die starke Behinderung der stationären Verdampfung ist. Unsere numerischen Berechnungen für die Verdampfung/Kondensation von Methylalkohol bestätigen die qualitative und quantitative Brauchbarkeit des Modells der kritischen Übersättigung für diese Art von Problemen, vorausgesetzt, dass die Voraussagen der kritischen Übersättigung auf grossen volumetrischen Keimbildungsgeschwindigkeiten beruhen. Entsprechend unseren Zielen ist die vorliegende Untersuchung begrenzt auf binäre Gasmischungen mit (1) einer Lewis-Zahl von 1 und (2) gleichem Molekulargewicht der beiden Komponenten. Da Methylalkohol–Luft-Gemische diesen Bedingungen gut entsprechen und für Forschung und Technologie interessant sind, werden für dieses System numerische Ergebnisse angegeben.

УСКОРЕНИЕ ПАРООБРАЗОВАНИЯ, ОГРАНИЧЕННОГО ДИФФУЗИЕЙ, ПУТЕМ КОНДЕНСАЦИИ В ПРЕДЕЛАХ ТЕРМИЧЕСКОГО ГРАНИЧНОГО СЛОЯ 2. СРАВНЕНИЕ ТЕОРИИ ГОМОГЕННОГО ЗАРОДЫШЕОБРАЗОВАНИЯ С МОДЕЛЬЮ КРИТИЧЕСКОГО ПЕРЕСЫЩЕНИЯ

Аннотация—Справедливость модели критического перенасыщения для расчета переноса массы при неравновесном образовании тумана в термических пограничных слоях исследуется путем сравнения расчетов, проведенных по модели критического перенасыщения с расчетами при более полном применении теории гомогенного образования пузырьков для случая течения с молекулярным переносом. Выражения для кинетики образования пузырьков и роста капель объединены со стационарными одномерными уравнениями непрерывности и преобразованы таким образом, чтобы для расчета испарения горячей конденсируемой фазы в холодную газовую среду можно было использовать цифровую вычислительную машину. С помощью одномерной пленочной модели термического пограничного слоя рассчитаны профили пограничного слоя и эффекты неравновесного образования тумана, и, как явствовало из модели критического перенасыщения, основным фактором, влияющим на образование тумана, было значительное увеличение стационарной скорости испарения. Наши численные расчеты испарения (конденсации) метилового спирта говорят о том, что модель критического перенасыщения можно использовать для расчета этого класса проблем на ЭЦВМ при условии больших значений объемных скоростей образования пузырьков. В соответствии с нашими целями настоящее исследование ограничивалось бинарными газовыми смесями с числом Льюиса, равным единице, и с равным молекулярным весом обоих компонентов смеси. Поскольку паровоздушные смеси метилового спирта, представляющие интерес для науки и техники, хорошо удовлетворяют этим ограничениям, для данной системы приводятся иллюстративные численные результаты.